Iranian Journal of Hydrogen & Fuel Cell 1(2022) 53-68

Iranian Journal of HYDROGEN & FUEL CELL

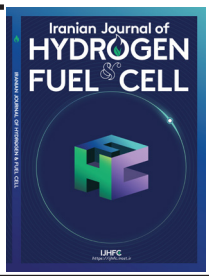

Thermodynamic and exergoeconomic evaluation of waste heat recovery for hydrogen production in a CCHP system

Armin Emamifar*

Mechanical Engineering Department, Ayatollah Boroujerdi University, Boroujerd, Iran

Article Information

Article History:

Received:
02 Mar 2022
Received in revised form:
13 Apr 2022
Accepted:
26 Apr 2022

Keywords

Kalina cycle
PEM electrolyzer
multigeneration
exergoeconomic analysis

Abstract

This study presents the energy, exergy, and economic evaluation of recovering energy from a modified Kalina power-cooling system to provide heating and hydrogen. An ORC is employed to use the waste heat of the Kalina cycle, and the generated power is transmitted to a PEM electrolyzer for hydrogen production. Furthermore, the waste heat of the separator outlet is recovered through a new heat exchanger to provide heating. The results show that the proposed system can produce 317 kW power, 714.7 kW cooling, 50.3 kW heating, and 4.491 kg/h hydrogen. Moreover, the exergoeconomic analysis indicates that the PEM electrolyzer, the cascade heat exchanger, and the vapor generator have the highest cost rate among the system components. Additionally, a parametric study was performed on the system to investigate the variation of some key parameters, including the maximum operating pressure, separator II pressure, ammonia mass fraction in a basic solution, and pinch point temperature difference in the cascade heat exchanger for the thermodynamic and economic performance of the system.

1. Introduction

In recent decades, the use of renewable energies and the recovery of waste energies have been increasingly studied due to industrial development, population growth, growing energy demand, depletion of fossil fuels, and attention to environmental impacts [1-3]. Hydrogen is clean energy that can be produced from water by electrolyzers. Moreover, hydrogen creates high energy and has the potential to be a promising

*Corresponding Author: emamifar@abru.ac.ir

doi: 10.22104/IJHFC.2022.5535.1237

energy carrier. Many studies have been done to make hydrogen by introducing more efficient and more economical thermodynamic systems [4, 5]. Kianfard et al. [6] used geothermal energy to drive a dual fluid ORC. The power generated by the high-pressure turbine of the ORC was used to run a RO distillation unit and a PEM electrolyzer to produce distilled water and hydrogen. The mass flow rate of hydrogen and distilled water obtained was 15.9 kg/h and 205.1 m^3/h, respectively. Nami et al. [7] used the waste heat of a gas turbine modular helium reactor in an ORC to generate power for hydrogen production and investigated the effect of several significant parameters on the system performance. They found that significant hydrogen can be produced through the waste heat recovery of the GTMHR by an ORC. The hydrogen production rate and exergy efficiency were reported at 56.2 kg/h and 49.21%, respectively. Yosaf and Ozcan [8] coupled an advanced absorption power system with a PEM electrolyzer for hydrogen production; their results demonstrated that their system could produce 1.5 kg hydrogen and 4.59 kg oxygen per day at maximum cycle temperature. They used an ejector to utilize more water vapor in the turbine and generate more power. The energy and exergy efficiencies obtained were 5.9% and 17.8 %, respectively. Moreover, their results showed that the turbine and the PEM electrolyzer had a higher cost rate than other system components. Nami et al. [9] employed an ORC to recover the waste heat of a molten carbonate fuel cell. The power generated by the ORC turbine was used to drive a PEM electrolyzer for hydrogen production. They revealed that more than 10 kg/h of hydrogen could be produced by the proposed system in some cases.

Bamisile et al. [10] presented a multigeneration system in which a concentrated photovoltaic system was integrated with an absorption system, a Kalina cycle, and a PEM electrolyzer. The presented system could produce electricity, a cooling effect, hot water, hot air, and hydrogen. The effect of the Kalina cycle was also investigated. The results showed that integration of the Kalina cycle could increase the system exergy efficiency from 68.73% to 70.08%. Kursun and Okten [11] used a photovoltaic thermal system and a flat plate solar collector to produce heat energy which was then converted to electrical energy through a Rankine cycle with ammonia working fluid. The electrical energy was delivered to a PEM electrolyzer for hydrogen production. Their results indicated that using the concentrated photovoltaic system can increase hydrogen production from 0.02 kg/h to 0.3 kg/h. Ni et al. [12] investigated the energy and exergy performance of a PEM electrolyzer and reported the effect of operating temperature, current density, electrolyzer thickness, and electrode catalytic activity on system performance. They concluded that a thin PEM electrolyte and higher operating temperatures can maximize the energy efficiency of the plant.

Ahmadi et al. [13] studied hydrogen production by coupling an ocean thermal energy conversion system with a solar-enhanced PEM electrolyzer. After passing a solar collector, the warm seawater provided heat energy for an ORC which used pure ammonia as working fluid. The electrical power generated by the ORC turbine was delivered to a PEM electrolyzer for hydrogen production. The energy efficiency, exergy efficiency, and hydrogen production rates obtained were 36%, 22.7%, and 1.2 kg/h, respectively. Sun et al. [14] investigated hydrogen production using a solar transcritical carbon dioxide power cycle to supply the required electrical energy for a PEM electrolyzer. Because an LNG was used in the condenser, a refrigeration heat exchanger was inserted in the cycle. The system's cold energy and hydrogen production rates were reported as 2.1 L/s and 11.52 kW, respectively. Fan et al. [15] studied the combination of a dual pressure ORC and PEM electrolyzer for power and hydrogen production. They used zeotropic mixtures in the ORC as working fluid and reported the maximum hydrogen production, energy efficiency, and exergy efficiency as 0.37 kg/h, 16.67%, and 58.14%, respectively.

Musharavati et al. [16] investigated the exergy and

exergoeconomic analysis for a hybrid system consisting of a low-grade ORC, an absorption system, and a PEM electrolyzer. They showed that 77% of total exergy destruction was produced in the generator, heat exchanger, and PEM electrolyzer. Furthermore, the energy and exergy efficiencies of the system obtained were 41% and 50%, respectively. Chitgar and Moghimi [17] presented a hybrid system that employed a solid oxide fuel cell and a gas turbine as the main source of energy. Additionally, a Kalina cycle, an ORC, and an LNG turbine were used to recover the waste heat and produce hydrogen and freshwater. They applied exergy and exergoeconomic analysis to the system and considered different objective functions in the genetic algorithm for system optimization. In the present paper, the Kalina power-cooling cycle proposed by Wang et al. [18] was first modified by adding an ORC to the cycle to produce power by recovering the waste energy of the cycle. Then, the power generated by the ORC was delivered to a PEM electrolyzer for hydrogen production. Next, the water entering the PEM electrolyzer was pre-heated by absorbing some waste heat from the Kalina cycle. An additional heat exchanger was also placed in the outlet of the separator II to provide heating to increase the system's efficiency. Lastly, energy, exergy, and exergoeconomic analysis were carried out to evaluate the thermodynamic and economic performance of the system.

2. System description

Fig. 1 illustrates the schematic diagram of the proposed multi-generation system, which is a modified system based on the cycle proposed by Wang et al. [18]. The presented system consists of a CCHP subsystem based on the Kalina cycle, an ORC, and a PEM electrolyzer. In the Kalina cycle, the working fluid is an ammonia/water mixture that leaves the vapor generator in two-phase conditions after absorbing heat from the heat source. First, the two-phase ammonia/water solution enters separator I, where the solution is separated into ammonia-rich vapor and a weak ammonia/water solution. The ammonia-rich vapor expands in the turbine to generate power. Next, the turbine outlet in a second phase condition enters into the second separator to achieve a richer ammonia vapor. This high-temperature rich ammonia vapor delivers some heat to the ORC and passes through a heat exchanger before entering the condenser.

In the condenser, the ammonia vapor is first condensed into a saturated liquid. Then, the liquid passes through an expansion valve and enters the evaporator to achieve the desired cooling effect. The weak ammonia/water solution exiting separator II has a high temperature, so it is passed through a heat exchanger to reach the required heating effect. Next, the weak solution mixes with the outlet stream of the evaporator and enters condenser II. The condensed solution is pumped to the regenerator to recover some energy from the weak solution outlet of separator I and then enters the vapor generator. The ORC subsystem uses Isobutane as a working fluid. In the cascade heat exchanger, the liquid working fluid absorbs the waste heat from the Kalina cycle and becomes saturated vapor. Next, the saturated vapor expands in the turbine to produce power. The turbine outlet stream is condensed in the condenser, and the saturated liquid is pumped to the cascade heat exchanger. Finally, the power generated by the ORC is delivered to a PEM electrolyzer to supply the required energy for hydrogen production.

3. Mathematical modeling

This section presents the required equations for the simulation of the proposed system. The following assumptions are made to simplify system modeling:

-The system operates at a steady state.

- The pressure losses through the pipes and components are negligible.
- The isenthalpic process is considered in the expansion valves.
- The rich vapor and the weak solution outlets from the separators are saturated vapor and saturated liquid, respectively.
- The outlet streams of all condensers are saturated liquid.
- The air consists of 79% nitrogen and 21% oxygen.

Thermodynamic modeling is carried out by applying

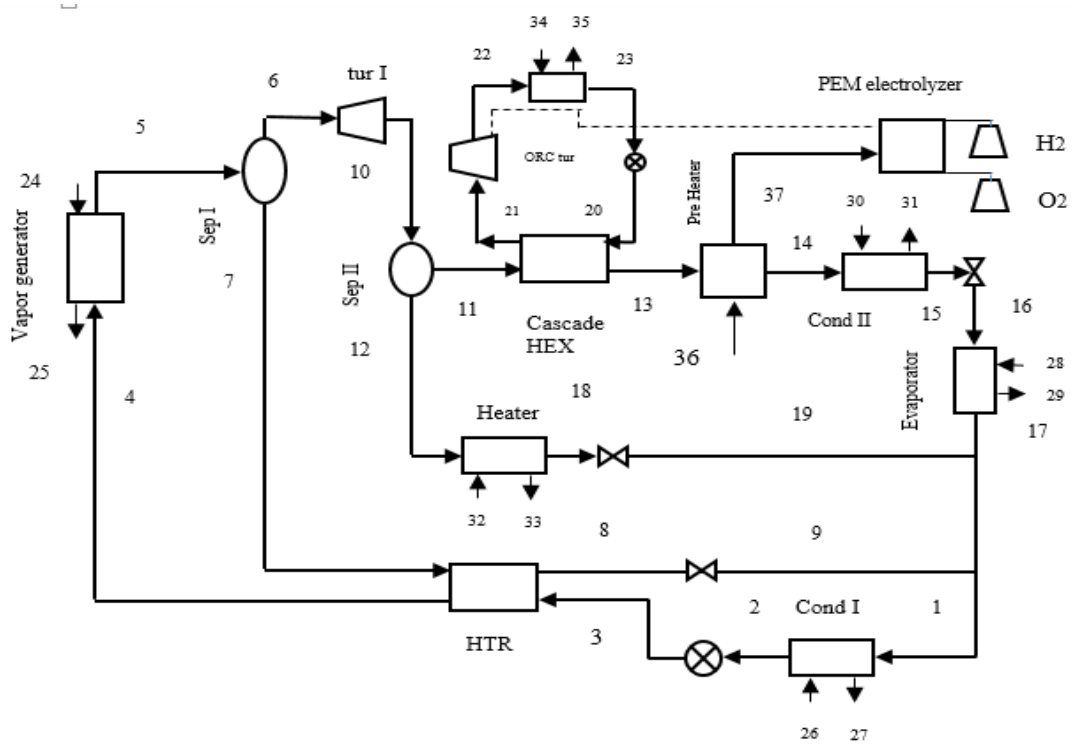

Fig. 1. Schematic diagram of the proposed system.

the mass balance, the energy conservation, and the exergy balance equation for each system component.

$$\sum \dot{m}_i - \sum \dot{m}_e = 0 \tag{1}$$

$$\sum \dot{m}_i h_i - \sum \dot{m}_e h_e + \sum \dot{Q} - \sum \dot{W} = 0 \tag{2}$$

$$\sum \dot{Q}_k \left(1 - \frac{T_0}{T_k}\right) + \sum \dot{m}_i ex_i = \sum \dot{m}_e ex_e + \sum \dot{W} + \dot{E}x_L \tag{3}$$

Where, $\dot{E}x_{D,k}$ is the exergy destruction rate. Moreover, $\sum \dot{Q}_k \left(1 - \frac{T_0}{T_k}\right)$ and $\sum \dot{W}$ are the exergy associated with heat transfer and power, respectively. The physical and chemical exergies are defined as follows:

$$ex_{ph} = \left(h - h_0\right) - T_0 \left(s - s_0\right) \tag{4}$$

$$ex_{ch} = \sum x_n ex_{ch,n} + RT_0 \sum x_n \ln x_n \tag{5}$$

$$ex = ex_{ph} + ex_{ch} \tag{6}$$

Where, x_n and $ex_{ch,n}$ denote the molar fraction and standard chemical exergy of each component, respectively. For the ammonia/water mixture, the chemical exergy can be calculated as follows:

$$e_{ch} = \left[\frac{e^0_{ch,NH_3}}{M_{NH_3}}\right] y + \left[\frac{e^0_{ch,H_2O}}{M_{H_2O}}\right] (1 - y) \tag{7}$$

Where, M_{NH3} and M_{H2O} are the molecular weights of ammonia and water, respectively, and y indicates the mass fraction of ammonia [19]. Applying fundamental equations (1-3) to all components of the proposed system, the energy and exergy equations for different components of the Kalina and ORC subsystems are given in Table 1.

Table 1. Exergy and Exergy Cost Balance Equations for the System Components

Component	Energy equation	Exergy equation
Kalina Turbine	$\dot{W}_{tur} = \dot{m}_6 (h_6 - h_{10})$	$\dot{E}x_6 = \dot{E}x_{10} + \dot{W}_{tur1} + \dot{E}_{D,tur1}$
Separator I	$\dot{m}_5 h_5 = \dot{m}_6 h_6 + \dot{m}_7 h_7$	$\dot{E}x_5 = \dot{E}x_6 + \dot{E}x_7 + \dot{E}_{D,SepI}$
Vapor generator	$\dot{Q}_{Vapor-generator} = \dot{m}_4 (h_5 - h_4)$ $\dot{Q}_{Vapor-generator} = \dot{m}_{source} (h_{24} - h_{25})$	$\dot{E}x_4 + \dot{E}x_{24} = \dot{E}x_5 + \dot{E}x_{25} + \dot{E}_{D,Vapor-generator}$
HTR	$\dot{Q}_{HTR} = \dot{m}_7 (h_7 - h_8) = \dot{m}_3 (h_4 - h_3)$	$\dot{E}x_7 + \dot{E}x_3 = \dot{E}x_8 + \dot{E}x_4 + \dot{E}_{D,HTR}$
Separator II	$\dot{m}_{10} h_{10} = \dot{m}_{11} h_{11} + \dot{m}_{12} h_{12}$	$\dot{E}x_{10} = \dot{E}x_{11} + \dot{E}x_{12} + \dot{E}_{D,SepII}$
Condenser I	$\dot{Q}_{Cond} = \dot{m}_1 (h_1 - h_2) = \dot{m}_{26} (h_{27} - h_{26})$	$\dot{E}x_1 + \dot{E}x_{26} = \dot{E}x_2 + \dot{E}x_{27} + \dot{E}_{D,CondI}$
Condenser II	$\dot{Q}_{CondII} = \dot{m}_{14} (h_{14} - h_{15}) = \dot{m}_{30} (h_{31} - h_{30})$	$\dot{E}x_{14} + \dot{E}x_{30} = \dot{E}x_{15} + \dot{E}x_{31} + \dot{E}_{D,CondII}$
Heater	$\dot{Q}_{Heater} = \dot{m}_{12} (h_{12} - h_{18}) = \dot{m}_{32} (h_{33} - h_{32})$	$\dot{E}x_{12} + \dot{E}x_{32} = \dot{E}x_{18} + \dot{E}x_{33} + \dot{E}_{D,Heater}$
Pump	$\dot{W}_{pump} = \dot{m}_2 (P_3 - P_2) / \rho \eta_p$ $\dot{W}_{pump} = \dot{m}_3 h_3 - \dot{m}_2 h_2$ $\dot{m}_3 = \dot{m}_2$	$\dot{E}x_2 = \dot{E}x_3 - \dot{W}_{Pump} + \dot{E}_{D,Heater}$
Pre-heater	$\dot{Q}_{Heater} = \dot{m}_{13} (h_{13} - h_{14}) = \dot{m}_{36} (h_{37} - h_{36})$	$\dot{E}x_{13} + \dot{E}x_{36} = \dot{E}x_{14} + \dot{E}x_{37} + \dot{E}_{D,\mathrm{Pr}e-heater}$
Throttling valve I	$h_{18} = h_{19}$	$\dot{E}x_{18} = \dot{E}x_{19} + \dot{E}_{D,VI}$
Throttling valve II	$h_{23} = h_{24}$	$\dot{E}x_{23} = \dot{E}x_{24} + \dot{E}_{D,VII}$
Evaporator	$\dot{Q}_{ref} = \dot{m}_{16} (h_{16} - h_{17}) = \dot{m}_{ref} (h_{29} - h_{28})$	$\dot{E}x_{16} + \dot{E}x_{28} = \dot{E}x_{17} + \dot{E}x_{29} + \dot{E}_{D,Evap}$
Cascade heat exchanger	$\dot{Q}_{Cas} = \dot{m}_{11} (h_{11} - h_{13}) = \dot{m}_{ORC} (h_{21} - h_{20})$	$\dot{E}x_{11} + \dot{E}x_{20} = \dot{E}x_{13} + \dot{E}x_{21} + \dot{E}_{D,Cas}$
ORC turbine	$\dot{W}_{ORC-tur} = \dot{m}_{ORC} (h_{21} - h_{22})$	$\dot{E}x_{21} = \dot{E}x_{22} + \dot{W}_{ORC-tur} + \dot{E}_{D,ORC-tur}$
ORC condenser	$\dot{Q}_{ORC-cond} = \dot{m}_{ORC} (h_{22} - h_{23})$ $\dot{Q}_{ORC-cond} = \dot{m}_{34} (h_{35} - h_{34})$	$\dot{E}x_{22} + \dot{E}x_{34} = \dot{E}x_{23} + \dot{E}x_{35} + \dot{E}_{D,ORC-Cond}$
ORC Pump	$\dot{W}_{ORC-pump} = \dot{m}_{ORC} (P_{20} - P_{23}) / \rho \eta_p$ $\dot{W}_{pump} = \dot{m}_{ORC} (h_{23} - h_{20})$	$\dot{E}x_{23} = \dot{E}x_{20} - \dot{W}_{ORC-Pump} + \dot{E}_{D,ORC-Pump}$

4. PEM electrolyzer modeling

The total energy required for the electrolyzer can be obtained as follows [7, 10, 12]:

$$\Delta H = \Delta G + T\Delta S \tag{8}$$

Where, DG and TDS are the Gibbs free energy and the required thermal energy, respectively. The PEM electrolyzer voltage can be calculated as follows:

$$V = V_0 + V_{Ohm} + V_{act,a} + V_{act,c} \tag{9}$$

Where, V_0 represents the reversible potential, V_{Ohm} denotes the ohmic overpotential, and $V_{act,a}$ and $V_{act,c}$ refer to the activation overpotential of the anode and cathode, respectively. The electrical energy input to the PEM electrolyzer is related to the PEM voltage through the following relation:

$$E_{electric} = JV \tag{10}$$

Where, J is the current density. Moreover, the mass flow rate of the produced hydrogen can be obtained as follows:

$$\dot{m}_{H_2,out} = \frac{J}{2F} \tag{11}$$

Where, F indicates the Faraday constant. The required equations for calculating the PEM electrolyzer voltage are presented in Table 2. According to the energy and exergy equations for each component, the overall energy and exergy efficiency of the system can be obtained as follows:

$$\eta_{overal} = \frac{\dot{W}_{tur} - \dot{W}_{pump} + \dot{Q}_{ref} + \dot{Q}_{heat} + \dot{m}_{H_2} LHV_{H_2}}{\dot{m}_{24}\left(h_{24} - h_{25}\right)} \tag{12}$$

$$\eta_{II,overal} = \frac{\dot{W}_{tur} - \dot{W}_{pump} + \left(Ex_{16} - Ex_{17}\right) + \left(Ex_{12} - Ex_{18}\right) + \dot{m}_{H_2} ex_{H_2}}{Ex_{24}} \tag{13}$$

Table 2. Electrochemical Equations for the PEM Electrolyzer [12, 13, 20, 21]

Parameter	Equation
Nernst Voltage	$V_0 = 1.229 - 8.5\times10^{-4}\left(T_{PEM} - 298\right)$
Anode Overpotential	$V_{act,a} = \frac{RT}{F}\sinh^{-1}\left(\frac{J}{2J_{0,a}}\right)$ $I_{0,a} = J_a^{ref}\exp\left(-\frac{E_{act,a}}{RT}\right)$ $E_{act,a} = 76(kJ/kmol), J_a^{ref} = 1.7\times10^5\left(Am^{-2}\right)$
Cathode Overpotential	$V_{act,c} = \frac{RT}{F}\sinh^{-1}\left(\frac{J}{2J_{0,c}}\right)$ $J_{0,c} = J_c^{ref}\exp\left(-\frac{E_{act,c}}{RT}\right)$ $E_{act,c} = 18(kJ/kmol), J_c^{ref} = 4.6\times10^3\left(Am^{-2}\right)$
Ohmic Overpotential	$V_{ohm} = JR_{PEM}$ $R_{PEM} = \int_0^D \frac{dx}{\sigma_{PEM}\left[\lambda(x)\right]}$ $\sigma_{PEM}\left[\lambda(x)\right] = \left[0.5139\lambda(x) - 0.326\right]\exp\left[1268\left(\frac{1}{303}\right.\right.$ $\lambda(x) = \frac{\lambda_a - \lambda_c}{D}x + \lambda_c$

5. Exergoeconomic analysis

In order to properly evaluate the system performance, an economic analysis should also be carried out. Exergoeconomic is a useful method that yields the cost per unit exergy for the system product streams. The

cost balance and appropriate auxiliary equation are applied to each system component in the exergoeconomic analysis.

$$\sum \dot{C}_{out,k} + \dot{C}_w = \sum \dot{C}_{in,k} + \dot{C}_Q + \dot{Z}_k \quad (14)$$

$$\dot{C} = c\dot{E}x \quad (15)$$

Where, C is the cost rate. The q and w indexes refer to the thermal exergy and power associated with the cost rates. Moreover, c is the cost per unit of exergy. Also, $\dot{Z}_k$ denotes the total system cost rate, including investment, operation, and maintenance costs for each component of the system.

$$\dot{Z}_k = \frac{Z_k CRF\varphi}{N} \quad (16)$$

Where, φ and N are the operation and maintenance factor and annual operation hours, respectively. Cost functions for the system components are displayed in Table 3. The parameter CRF denotes the capital recovery factor and can be calculated as:

$$CRF = \frac{i_r(1+i_r)^n}{(1+i_r)^n - 1} \quad (17)$$

Where, i_r indicates the interest rate and n refers to the plant's operation years. The specific cost of the fuel exergy ($c_{F,k}$) and the product exergy ($c_{P,k}$) for each component can be obtained as follows:

$$c_{P,k} = \frac{\dot{C}_{P,k}}{\dot{E}x_{P,k}} \quad (18)$$

$$c_{F,k} = \frac{\dot{C}_{F,k}}{\dot{E}x_{F,k}} \quad (19)$$

Moreover, the cost associated with exergy destruction can be expressed as:

$$\dot{C}_{D,k} = c_{F,k}\dot{E}x_{D,k} \quad (20)$$

Furthermore, the exergoeconomic factor that indicates the contribution of non-exergetic costs to the total cost of each component is defined as follows:

$$f_k = \frac{\dot{Z}_k}{\dot{Z}_k + \dot{C}_{D,k}} \quad (21)$$

The total cost rate for each subsystem is a summation of the operation and maintenance cost rate and the exergy destruction cost rate. Accordingly, the total cost rate of the system can be calculated as:

$$C_{total} = C_{Kalina} + C_{ORC} + C_{PEM} = \sum \dot{Z}_k + \sum \dot{C}_{D,k} \quad (22)$$

The cost balance equations and the needed auxiliary equations for each component of the system are displayed in Table 4.

Table 3. Cost Functions for the System Components [6, 8, 17]

Component	Cost function ($)
Turbine	$4750\left(\dot{W}_{tur}\right)^{0.75}$
Pump	$3500\left(\dot{W}_{Pump}\right)^{0.41}$
Electrolyzer	$1000\left(\dot{W}_{PEM}\right)$
HTR,HXE,Condenser	$309.14\left(A_{Cond}\right)^{0.85}$
Separator	$280.3\left(\dot{m}_{Seperator-inlet}\right)^{0.67}$

Table 4. Exergy Cost Balance Equations for the System Components

Component	Exergy cost balance equations
Kalina Turbine	$\dot{C}_6 + \dot{Z}_{tur} = \dot{C}_{10} + \dot{C}_{W,tur}$ $c_6 = c_{10}$
Separator I	$\dot{C}_5 + \dot{Z}_{SepI} = \dot{C}_6 + \dot{C}_7$ $c_6 = c_7$
Vapor generator	$\dot{C}_4 + \dot{C}_{24} + \dot{Z}_{Vg} = \dot{C}_5 + \dot{C}_{25}$ $c_{24} = c_{25}$
HTR	$\dot{C}_7 + \dot{C}_3 + \dot{Z}_{HTR} = \dot{C}_8 + \dot{C}_4$ $c_7 = c_8$
Separator II	$\dot{C}_{10} + \dot{Z}_{SepII} = \dot{C}_{11} + \dot{C}_{12}$ $c_{11} = c_{12}$
Condenser I	$\dot{C}_1 + \dot{C}_{26} + \dot{Z}_{CondI} = \dot{C}_2 + \dot{C}_{27}$ $c_{27} = 0$
Condenser II	$\dot{C}_{14} + \dot{C}_{30} + \dot{Z}_{CondII} = \dot{C}_{15} + \dot{C}_{31}$ $c_{31} = 0$
Heater	$\dot{C}_{12} + \dot{C}_{32} + \dot{Z}_{Heater} = \dot{C}_{18} + \dot{C}_{33}$ $c_{12} = c_{18}$
Pump	$\dot{C}_2 + \dot{C}_{W,Pump} + \dot{Z}_{Pump} = \dot{C}_3$ $\frac{\dot{C}_{W,Pump}}{\dot{W}_{pump}} = \frac{\dot{C}_{W,tur}}{\dot{W}_{tur}}$
Pre-heater	$\dot{C}_{13} + \dot{C}_{36} + \dot{Z}_{Pre-heater} = \dot{C}_{14} + \dot{C}_{37}$ $c_{13} = c_{14}$
Trottling valve I	$\dot{C}_{18} = \dot{C}_{19}$
Trottling valve II	$\dot{C}_{23} = \dot{C}_{24}$
Evaporator	$\dot{C}_{16} + \dot{C}_{28} + \dot{Z}_{Evap} = \dot{C}_{17} + \dot{C}_{29}$ $c_{16} = c_{17}$
PEM	$\dot{C}_{37} + \dot{C}_{W,PEM} + \dot{Z}_{PEM} = \dot{C}_{H_2}$ $\frac{\dot{C}_{W,PEM}}{\dot{W}_{PEM}} = \frac{\dot{C}_{W,ORC-tur}}{\dot{W}_{ORC-tur}}$
Cascade heat exchanger	$\dot{C}_{11} + \dot{C}_{20} + \dot{Z}_{Cas} = \dot{C}_{13} + \dot{C}_{21}$
ORC turbine	$\dot{C}_{21} + \dot{Z}_{ORC-tur} = \dot{C}_{22} + \dot{C}_{W,ORC-tur}$ $c_{21} = c_{22}$
ORC condenser	$\dot{C}_{22} + \dot{C}_{34} + \dot{Z}_{ORC-Cond} = \dot{C}_{23} + \dot{C}_{35}$ $c_{35} = 0$
ORC Pump	$\dot{C}_{23} + \dot{C}_{W,ORC-Pump} + \dot{Z}_{ORC-Pump} = \dot{C}_{20}$ $\frac{\dot{C}_{W,ORC-Pump}}{\dot{W}_{ORC-Pump}} = \frac{\dot{C}_{W,ORC-tur}}{\dot{W}_{ORC-tur}}$

6. Results and discussion

Energy, exergy, and exergoeconomic analysis were carried out for the proposed system. The input data used in the calculations are presented in Table 5. EES software was employed to perform all thermodynamic computations. The verification of the Kalina cycle was accomplished using the data reported in Ref [18]. A comparison of some key parameters (see Table 6) indicates a good coincidence with a maximum difference of 2.28%. Additionally, the obtained voltage of the electrolyzer was compared with the experimental results of the Ref [12] to verify the PEM electrolyzer modeling. As can be observed from Fig. 2, a good agreement exists between the two results.

Table 5. The Input Parameters of the System [3, 6, 12, 17, 18, 22]

Parameter	Value
Condenser cooling water input temperature	298 (K)
Mass flow rate of heat source	88.24 (kg/s)
Temperature of heat source	474 (K)
Pressure of heat source	1.5 (bar)
Kalina turbine inlet temperature	453 (K)
Kalina turbine inlet pressure	20 (bar)
Kalina turbine back pressure	7 (bar)
Concentration of basic solution	0.28
Temperature difference in HTR	10 (K)
Evaporator pressure	0.7 (bar)
Evaporator outlet temperature	288 (K)
Temperature difference in cascade heat exchanger	10 (K)
ORC condenser pressure	3.713 (bar)
PEM temperature	353 (K)
$л_a$	14
$л_c$	10
D	50 (μm)
$E_{act,a}$	76 (kJ/mol)
$E_{act,c}$	18 (kJ/mol)
Faraday constant	96490 (C/mol)
Ambient temperature	293.15 (K)
Ambient pressure	1 (bar)
Turbine isentropic efficiency	85%
Pump isentropic efficiency	70%
Compressor isentropic efficiency	85%
Maintenance factor	1.06
Discount rate	0.14
System lifetime	15 (years)
Operating hours per year	7300

Table 6. Comparison of Kalina Cycle Parameters with Ref [18]

Parameter	Present model results (kW)	Ref [18] model results (kW)	Error (%)
$\dot{W}_{turbine}$	38.28	37.63	1.72
$\dot{W}_{Pump}$	1.79	1.75	2.28
$\dot{Q}_{ref}$	75.53	75.12	0.54
η_{th}	13.83	13.72	0.87
η_{II}	5.46	5.40	1.11

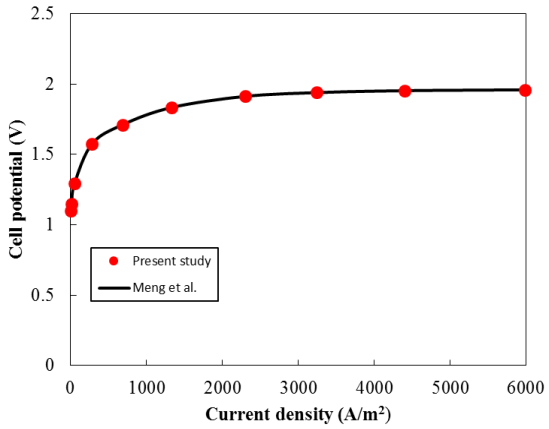

Fig. 2. Verification of the PEM electrolyzer simulation.

Table 7 represents the calculated parameters related to the energy and exergy of the proposed system. As displayed in Table 5, the presented system can produce a net power of 317 kW through the Kalina cycle. Moreover, 714.7 kW of the cooling load and 50.3 kW of the heating load can be achieved from the system. Additionally, by recovering the waste heat in the ORC, 263.6 kW of power can be generated to produce 4.491 kg/h of hydrogen through the PEM electrolyzer.

Table 7. Energy and Exergy Parameters of the Proposed System

Parameter	Value
$\dot{W}_{Kalina}$ (kW)	317
$\dot{W}_{ORC}$ (kW)	263.6
$\dot{Q}_{ref}$ (kW)	714.7
$\dot{Q}_{heat}$ (kW)	50.3
$\dot{m}_{H_2}$ (kg/hr)	4.491
η_{Overal} (%)	30.46
$\eta_{II,Overal}$ (%)	22.04

The exergoeconomic results for different components of the system are reported in Table 8. As can be observed, the Kalina turbine and the ORC turbine have the highest exergoeconomic factor, which indicates that the investment costs of these components are higher than the cost related to exergy destruction. Moreover, the heat exchangers and the separators have a lower exergoeconomic factor which shows that the costs related to exergy destructions are more prominent in these components. Besides, as can be found in Table 8, the vapor generator, the cascade heat exchanger, and the PEM electrolyzer have higher values of $\dot{Z}_k + \dot{C}_{D,k}$, which illustrates that more attention should be paid to these components.

Table 8. Exergoeconomic Results for the Proposed System

Component	$\dot{E}_{D,k}(kW)$	$\dot{Z}_k(\$/h)$	$\dot{C}_{D,k}(\$/h)$	$\dot{Z}_k + \dot{C}_{D,k}(\$/h)$	$f_k(\%)$
Kalina Turbine	43.46	8.712	3.671	12.383	70.35
Vapor Generator	339.4	1.663	19.08	20.743	8.01
HTR	89.07	0.931	13.77	14.701	6.33
Condenser I	47.81	1.158	4.04	5.198	22.22
Condenser II	196.3	0.7841	16.44	17.2241	4.55
Evaporator	22.32	0.8312	1.874	2.7052	30.73
Heater	8.49	0.075	0.71	0.785	9.62
Pre heater	40.75	0.2569	3.41	3.6669	6.99
Separator I	100.9	0.019	8.49	8.509	0.22
Separator II	10.48	0.01045	0.885	0.8954	1.16
Pump	3.26	0.2364	0.31	0.5464	43.12
PEM	117.5	6.231	19.98	26.211	23.77
Cascade heat exchanger	234	0.6791	19.6	20.2791	3.34
ORC turbine	47.05	7.67	6.84	14.51	52.84
ORC condenser	30.9	1.53	4.496	6.026	25.42
ORC pump	3.11	0.25	0.53	0.78	31.94

Fig. 3 shows the effect of the maximum pressure of the Kalina cycle on the total system performance. By increasing the maximum pressure, the mass flow rate of the vapor exiting the separator I decreases. As a result, the enthalpy drop across the turbine also increases, which leads to an increase in the Kalina turbine's power. An upward trend can be observed in the output power after increasing the pressure in separator I from 18 bar to 28 bar, and the quality of the ammonia solution entering separator II decreases, which causes a decrease in the mass flow rate of the saturated ammonia vapor generated in separator II. Conversely, increasing the maximum pressure of the Kalina cycle increases the ammonia mass fraction in the ammonia vapor outlet of the separator II. Hence, the specific enthalpy of the ammonia solution entering the evaporator decreases. The increase of enthalpy difference through the evaporator overcomes the decrease in the ammonia mass flow rate and the refrigeration capacity increases. Furthermore, reducing the ammonia mass flow rate exiting separator II decreases the heat transfer to the ORC, decreasing the ORC output power. Therefore, the hydrogen production decreases; however, the heating capacity increases due to the increase in the mass flow rate of the saturated liquid exiting the separator II. As can be observed from Fig 3.b, the total cost rate of the system decreases when the maximum pressure of the Kalina cycle increases.

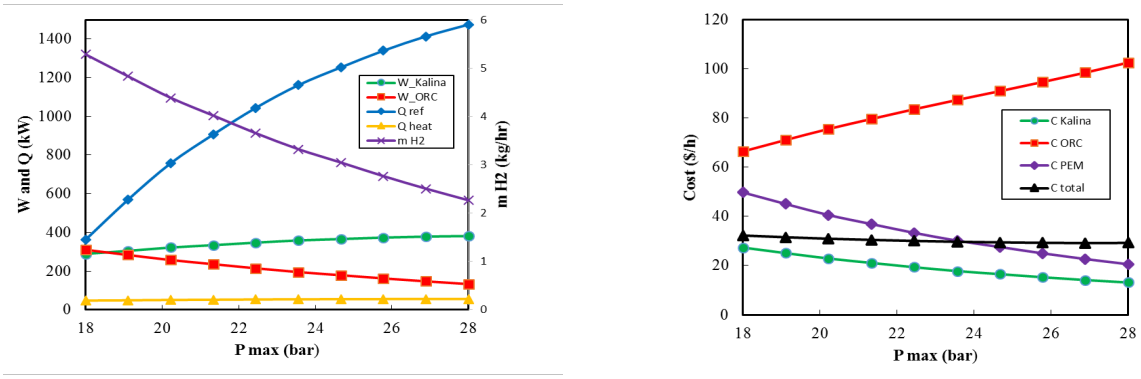

(a) (b)

Fig. 3. Effect of variations of maximum pressure of the Kalina cycle on a) thermodynamic performance of the cycle, b) total cost rates.

Fig. 4 represents the effect of the pressure in separator II on the total system performance. By increasing the pressure in separator II, the quality and specific enthalpy of the ammonia solution exiting the Kalina turbine increases, which leads to a decrease in the output power of turbine I. Moreover, by increasing the quality of the ammonia solution entering separator II, the mass flow rate of the saturated ammonia vapor generated in separator II increases. However, decreasing the mass fraction of ammonia leads to a decrease in the refrigeration capacity of the system. As can be seen from Fig. 2b, the ORC output power and H2 production increase as the pressure in separator II increases. This is because increasing the pressure in separator II increases the specific enthalpy of the saturated vapor generated in separator II. Therefore, the heat transferred to the ORC increases, which leads to an increase in the output power of the ORC turbine. Furthermore, the heating capacity decreases by decreasing the mass flow rate of the saturated liquid solution exiting the separator II. Although increasing the pressure in separator II causes a decrease in the total cost rate of the Kalina cycle, the increase in the total cost rate of the ORC and PEM electrolyzer is dominant. Hence, the total cost rate of the system increases when the pressure in separator II increases.

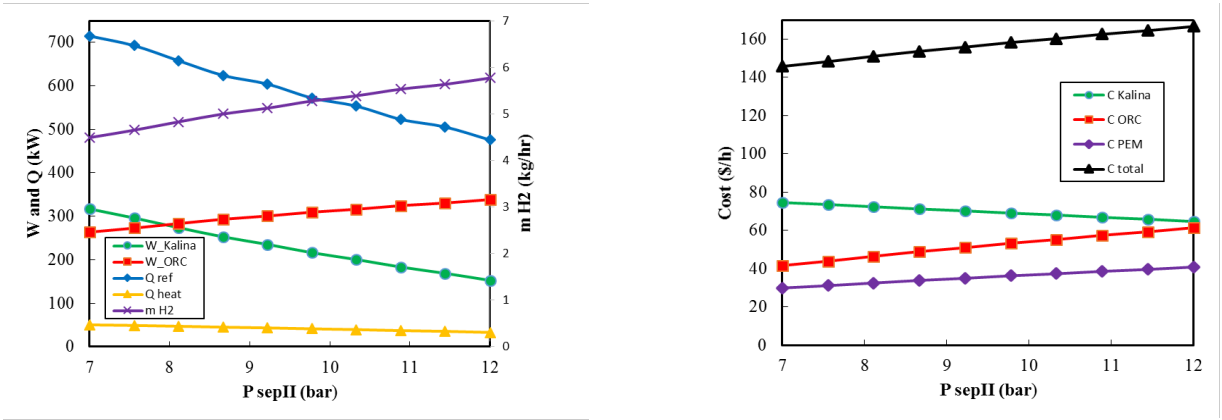

(a) (b)

Fig. 4. Effect of variations of pressure in separator II on a) thermodynamic performance of the cycle, b) total cost rates.

The effects on the total system performance of varying the ammonia mass fraction of the basic solution are illustrated in Fig. 5. By increasing the ammonia mass fraction of the basic solution, the mass flow rate of ammonia vapor exiting separator I and, consequently, the mass flow rates of the outlet streams of separator II increase. Moreover, by increasing the heat transfer to the ORC, the output power of the ORC turbine, the rate of hydrogen production, the refrigeration capacity, and the heating capacity of the system increase. However, due to low pressure in the condenser, the temperature at the Kalina condenser decreases so that a cooling system will be needed to perform condensation at higher ammonia mass fractions of the basic solutions. Therefore, ammonia mass fractions higher than 0.28 are not recommended for the proposed conditions. The total cost rate of the system remains almost constant due to little change in the total system performance.

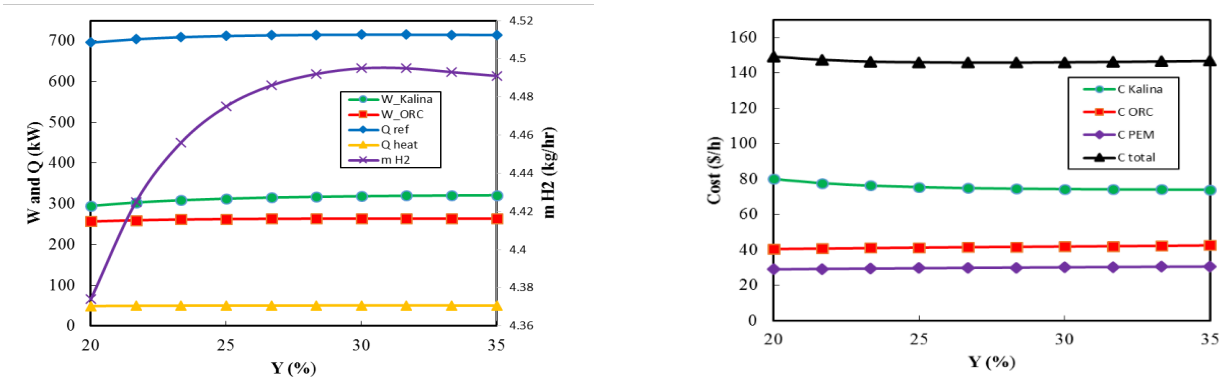

(a) (b)

Fig. 5. Effect of variations of ammonia mass fraction of basic solution on a) thermodynamic performance of the cycle, b) total cost rates.

Fig. 6 represents the effect of the pinch point temperature difference in the cascade heat exchanger on the system performance. As shown in Fig. 4a, variations of DT_P do not change the Kalina cycle power, refrigeration capacity, or heating capacity of the system because the heat transferred from the Kalina cycle to the ORC is waste energy. Therefore, the performance of the Kalina cycle remains constant. On the other hand, increasing the DT_P decreases the heat transfer to the ORC, which reduces the output power and the hydrogen production rate, slightly increasing the total cost rate of the system. Increasing the DT_P causes to decrease in the maximum temperature of the ORC. Hence, the performance of the ORC declines, and the cost rates of the ORC cycle increase. Furthermore, the cost rate of the Kalina cycle and the PEM electrolyzer remain constant, so increasing the ORC cost rate increases the cost rate of the system.

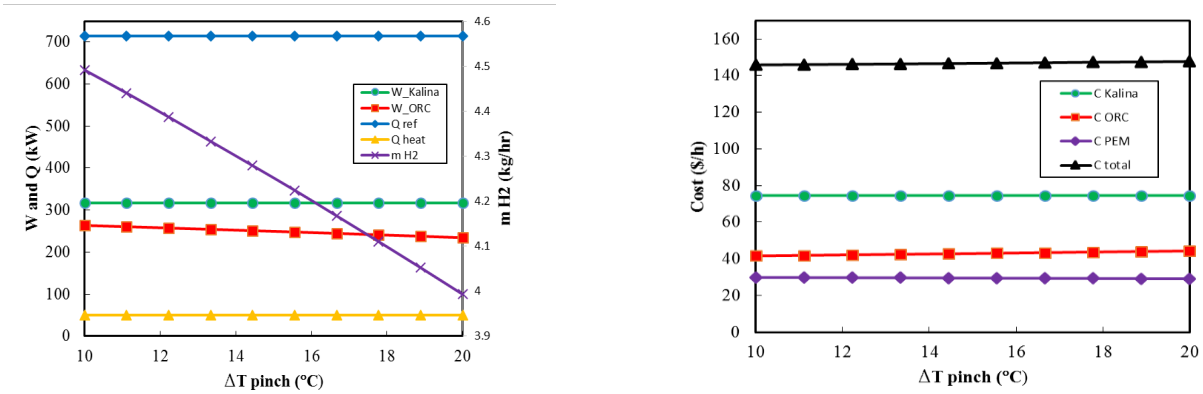

(a) (b)

Fig. 6. . Effect of variations of pinch point temperature difference in the cascade heat exchanger on a) thermodynamic performance of the cycle, b) total cost rates.

7. Conclusion

This study evaluated the recovery of the waste energy of a Kalina power-cooling system to provide heating and hydrogen production. Using the waste heat of the Kalina cycle, an ORC was employed to produce the power required for hydrogen production by a PEM electrolyzer. Moreover, the waste heat of the separator II outlet was also recovered by another heat exchanger to provide heating. The most important results of this study can be summarized as follows:

- The system produced 317 kW power, 714.7 kW cooling, 50.3 kW heating, and 4.491 kg/h hydrogen.
- The PEM electrolyzer, the cascade heat exchanger, and the vapor generator have the highest cost rate among the system components.
- Increasing the pressure in separator II and the ammonia mass fraction in the basic solution increases the hydrogen production rate. However, the hydrogen production ratedecreases as the maximum operating pressure of the cycle and pinch point temperature difference in the cascade heat exchanger increase.
- Total cost rate of the system increases as the maximum operating pressure of the cycle and pinch point temperature difference in the cascade heat exchanger increase.
- The generated power, the cooling effect, and the heating effect increase as the maximum pressure of the cycle and ammonia mass fraction in the basic solution increase.

Nomenclature

c	Cost per unit exergy ($/GJ)	Greek letter	
$\dot{C}$	Cost rate ($/h)	η	Energy efficiency
CRF	Capital recovery factor	η_{II}	Exergy efficiency
cond	Condenser	$\lambda(x)$	water content at location x in the membrane (molH_2O/molSO_3^-)
$E_{act,a}$	activation energy in anode (kJ)	λ_a	water content at the anode-membrane interface (molH_2O/molSO_3^-)
$E_{act,c}$	activation energy in cathode (kJ)	λ_c	water content at the cathode-membrane interface (molH_2O/molSO_3^-)
$\dot{E}x$	Exergy rate (kW)	y	Ionic conductivity (s/m)
ex	Specific exergy (kJ/kg)	Subscripts	
F	Faraday constant (C/mol)	act	Activation
f	Exergoeconomic factor	ch	chemical
G	Gibbs free energy (J/mol)	D	destruction
h	Specific enthalpy (kJ/kg)	H_2	Hydrogen
HTR	high-temperature recuperator	H_2O	Water
HEX	Heat exchanger	O_2	Oxygen
J	Current density (A/m2)	ph	Physical
J_0	exchange current density (A/m2)	sat	Saturation
J_i^{ref}	pre-exponential factor (A/m2)	tur	Turbine
LHV	Low heating value		
$\dot{m}$	Mass flow rate (kg/s)		
N	Annual plant operation hours (h)		
ORC	Organic Rankine cycle		
P	Pressure (bar)		
s	Specific entropy (kJ/kgK)		
T	Temperature (K)		
V	Voltage (V)		
$\dot{Z}$	Cost rate of components ($/h)		
V_0	reversible potential (V)		
$V_{act,a}$	anode activation overpotential (V)		
$V_{act,c}$	cathode activation overpotential (V)		
V_{Ohm}	ohmic overpotential (V)		
$\dot{W}_{Kalina}$	net power of the Kalina cycle (kW)		
$\dot{W}_{ORC}$	net power of the ORC cycle (kW)		

References

[1] E. Akrami, A. Nemati, H. Nami, F. Ranjbar, Exergy and exergoeconomic assessment of hydrogen and cooling production from concentrated PVT equipped with PEM electrolyzer and LiBr-H2O absorption chiller, *International Journal of Hydrogen Energy,* 43(2), 622-633, 2018.

[2] J. Han, X. Wang, J. Xu, N. Yi, S. S. Ashraf Talesh, Thermodynamic analysis and optimization of an innovative geothermal-based organic Rankine cycle using zeotropic mixtures for power and hydrogen production, *International Journal of Hydrogen Energy,* 45(15), 8282-8299, 2020.

[3] N. Sarabchi, S. M. S. Mahmoudi, M. Yari, A. Farzi, Exergoeconomic analysis and optimization of a novel hybrid cogeneration system: High-temperature proton exchange membrane fuel cell/Kalina cycle, driven by solar energy, *Energy Conversion and Management,* 190, 14-33, 2019.

[4] M. Ni, M. K. H. Leung, K. Sumathy, D. Y. C. Leung, Potential of renewable hydrogen production for energy supply in Hong Kong, *International Journal of Hydrogen Energy,* 31(10), 1401-1412, 2006.

[5] J. Nowotny, T. Hoshino, J. Dodson, A. J. Atanacio, M. Ionescu, V. Peterson, K. E. Prince, M. Yamawaki, T. Bak, W. Sigmund, T. N. Veziroglu, M. A. Alim, Towards sustainable energy. Generation of hydrogen fuel using nuclear energy, *International Journal of Hydrogen Energy,* Vol. 41(30), 12812-12825, 2016.

[6] H. Kianfard, S. Khalilarya, S. Jafarmadar, Exergy and exergoeconomic evaluation of hydrogen and distilled water production via combination of PEM electrolyzer, RO desalination unit and geothermal driven dual fluid ORC, *Energy Conversion and Management,*177, 339-349, 2018.

[7] H. Nami, F. Mohammadkhani, F. Ranjbar, Utilization of waste heat from GTMHR for hydrogen generation via combination of organic Rankine cycles and PEM electrolysis, *Energy Conversion and Management,* 127, 589-598, 2016.

[8] S. Yosaf, H. Ozcan, Exergoeconomic investigation of flue gas driven ejector absorption power system integrated with PEM electrolyser for hydrogen generation, *Energy,* 163, 88-99, 2018.

[9] H. Nami, E. Akrami, F. Ranjbar, Hydrogen production using the waste heat of Benchmark pressurized Molten carbonate fuel cell system via combination of organic Rankine cycle and proton exchange membrane (PEM) electrolysis, *Applied Thermal Engineering,* 114, 631-638, 2017.

[10] O. Bamisile, Q. Huang, M. Dagbasi, V. Adebayo, E. C. Okonkwo, P. Ayambire, T. Al-Ansari, T. A. H. Ratlamwala, Thermo-environ study of a concentrated photovoltaic thermal system integrated with Kalina cycle for multigeneration and hydrogen production, *International Journal of Hydrogen Energy,* 45(51), 26716-26732, 2020.

[11] B. Kurşun, K. Ökten, Thermodynamic analysis of a Rankine cycle coupled with a concentrated photovoltaic thermal system for hydrogen production by a proton exchange membrane electrolyzer plant, *International Journal of Hydrogen Energy,* 44(41),22863-22875, 2019.

[12] M. Ni, M. K. H. Leung, D. Y. C. Leung, Energy and exergy analysis of hydrogen production by a proton exchange membrane (PEM) electrolyzer plant, *Energy Conversion and Management,* 49(10), 2748-2756, 2008.

[13] P. Ahmadi, I. Dincer, M. A. Rosen, Energy and exergy analyses of hydrogen production via solar-boosted ocean thermal energy conversion and PEM electrolysis, *International Journal of Hydrogen Energy,* 38(4), 1795-1805, 2013.

[14] Z. Sun, J. Wang, Y. Dai, J. Wang, Exergy analysis and optimization of a hydrogen production process by a solar-liquefied natural gas hybrid driven transcritical CO2 power cycle, *International Journal of Hydrogen Energy,* 37(24), 18731-18739, 2012.

[15] G. Fan, B. Yang, P. Guo, S. Lin, S. G. Farkoush, N. Afshar, Comprehensive analysis and multi-objective optimization of a power and hydrogen production system based on a combination of flash-binary geothermal and PEM electrolyzer, *International Journal of Hydrogen Energy,* 46(68), 33718-33737, 2021.

[16] F. Musharavati, P. Ahmadi, S. Khanmohammadi, Exergoeconomic assessment and multiobjective optimization of a geothermal-based trigeneration system for electricity, cooling, and clean hydrogen production, *Journal of Thermal Analysis and Calorimetry,* 145(3), 1673-1689, 2021.

[17] N. Chitgar, M. Moghimi, Design and evaluation of a novel multi-generation system based on SOFC-GT for electricity, fresh water and hydrogen production, *Energy,* 197, 117162, 2020.

[18] J. Wang, J. Wang, P. Zhao, Y. Dai, Thermodynamic analysis of a new combined cooling and power system using ammonia–water mixture, *Energy Conversion and Management,* 117, 335-342, 2016.

[19] J. Szargut, *Exergy Method: Technical and Ecological Applications*: WIT Press, 2005.

[20] C. Lamy, From hydrogen production by water electrolysis to its utilization in a PEM fuel cell or in a SO fuel cell: Some considerations on the energy efficiencies, *International Journal of Hydrogen Energy,* 41(34),15415-15425, 2016.

[21] J. A. Salva, A. Iranzo, F. Rosa, E. Tapia, Validation of cell voltage and water content in a PEM (polymer electrolyte membrane) fuel cell model using neutron imaging for different operating conditions, *Energy,* 101, 100-112, 2016.

[22] F. I. Abam, T. A. Briggs, O. E. Diemuodeke, E. B. Ekwe, K. N. Ujoatuonu, J. Isaac, M. C. Ndukwu, Thermodynamic and economic analysis of a Kalina system with integrated lithium-bromide-absorption cycle for power and cooling production, *Energy Reports,* 6, 1992-2005, 2020.